Published in final edited form as:
Biochemistry. 2008 June 24; 47(25): 6719–6726. doi:10.1021/bi800309m.

Biochemical Analysis of MST1 Kinase: Elucidation of a C-Terminal Regulatory Region[†]

Ruchi Anand[‡], **Ah-Young Kim**[§], **Michael Brent**[‡,§], and **Ronen Marmorstein**[*,‡,§]
The Wistar Institute, 3601 Spruce Street, Philadelphia, Pennsylvania 19104, and Department of Chemistry, University of Pennsylvania, Philadelphia, Pennsylvania 19104

Abstract

The MST1 kinase phosphorylates FoxO transcription factors in the cytosol and histone H2B in the nucleus to promote cellular apoptosis. In addition to a N-terminal kinase domain, MST1 contains C-terminal regulatory and dimerization regions that are cleaved upon nuclear transport. In this report, we investigate the role of the MST1 regulatory region and dimerization domain in MST1 activity toward FoxO and histone H2B substrates. We find that the MST1 regulatory region enhances FoxO phosphorylation while inhibiting histone H2B phosphorylation, consistent with the cellular properties of MST1. We also identify autophosphorylation sites within the MST1 regulatory region and show that both regulatory region phosphorylation and MST1 dimerization contribute to FoxO phosphorylation. Together, our studies provide new insights into how MST1 substrate selectivity is modulated with implications for understanding apoptotic signaling through MST1 kinase.

The MST1[1] kinase was first isolated by Krebs and coworkers in 1998 as a 36 kDa protein from mammalian cells that are activated by severe stress induced by okadaic acid and staurosporine (1). The MST proteins belong to a large family of serine/threonine kinases called sterile 20 proteins (Ste20p) (2) that contains at least 35 members (3). All members of the Ste20 family contain a conserved kinase domain and a structurally diverse region, which is implicated in regulation (3). On the basis of their domain architecture, the Ste20 group is further divided into two distinct families, PAK1 (p21-activated kinase) (4) and GCK (human germinal center). The two families are distinguished by the relative positions of their kinase domains with the PAKs containing a C-terminal kinase domain and the GCKs, including MST1, containing an N-terminal kinase domain. MST1 is 487 amino acids long and also contains a C-terminal regulatory domain and an extreme 56-residue C-terminal α-helical domain implicated in homodimerization (5).

MST1 is a proapoptotic cytosolic kinase (6). Activation of MST1 via the caspase 3 pathway leads to apoptosis (7), and overexpression of MST1 results in the induction of apoptosis in a variety of cell backgrounds through pathways that involve activation of SAPK (stress-activated protein kinase) (7). Upon activation of the apoptotic pathway, MST1 is cleaved by caspase-3

[†]This work was supported by a National Institutes of Health grant to R.M.

* To whom correspondence should be addressed. E-mail: marmor@wistar.org. Phone: (215) 898-5006. Fax: (215) 898-0381.
[‡]The Wistar Institute,
[§]University of Pennsylvania.

SUPPORTING INFORMATION AVAILABLE: Autoradiography of MST1 (Figure S1), autoradiography of mutant MST1 constructs (Figure S2), and phosphoactivation of activation loop threonine 183 (Figure S3). This material is available free of charge via the Internet at http://pubs.acs.org.

[1]Abbreviations: MST1, mammalian sterile 20; MST1-FL, MST1 full-length; KD, kinase domain; RR, regulatory domain; DD, dimerization domain; PAK1, p21-activated kinase; Ste20p, sterile 20 protein; GCK, human germinal center; SAPK, stress-activated protein kinase; CST, *Caenorhabditis elegans* sterile 20; SUMO, small ubiquitin-related modified; NORE, novel Ras effector; AU, analytical ultracentrifugation.

at a conserved recognition motif (DEMD^{326}) (8), resulting in its translocation to the nucleus. MST1 also contains a site (TMTD^{349}) whose cleavage by caspase-6/7 yields an active 41 kDa fragment (9).

The mechanism of MST1 regulation has been a subject of investigation for quite some time (10,11). Studies by Rezka and co-workers using mouse lysates overexpressing MST1 in 293 cells investigated the role of phosphorylation sites and found that two residues, T183 and T187, within the activation loop of the kinase domain have a marked influence on enzyme activation, with mutation of T183 to alanine abrogating MST1 activation. This is comparable with inhibition caused by mutating K59R at the MST-ATP binding site (11), which is known to retain only 1% of its activity. Two protein substrates for MST1 have been identified. In 2003, Allis and co-workers demonstrated that MST1 phosphorylates histone 2B at serine 14 (12). Histone 2B is a component of the fundamental unit of eukaryotic chromatin, the nucleosome (13). Various histone post-transitional modifications such as acetylation, phosphorylation, and methylation influence chromatin function (14). In mammalian cells, the only core histone modification that has been associated with apoptosis is histone 2B phosphorylation (15). Allis and co-workers (12) demonstrated that H2B phosphorylation at Ser14 specifically correlates with the onset of apoptosis in human HL-60 cells. Phosphorylation of H2B at Ser14 has also been shown to be correlated with programmed cell death during *Xenopus* tail resorption (12). A more recent report demonstrates that MST1 kinase also catalyzes the phosphorylation of FOXO transcription factors at a conserved serine within the DNA binding domain (16). The FOXO proteins have a conserved winged-helix DNA binding domain which is a signature of the FOX family of proteins (17). The FoxO proteins mediate their activities by binding to DNA through their forkhead DNA binding domain and activating or repressing the expression of specific groups of target genes in response to cellular conditions. FoxO activity has been shown to be regulated by a number of post-translational modifications, and misregulation of these post-translational modifications has been proposed to play a key role in the regulation of diseases of aging (18). MST1-induced phosphorylation of FoxO disrupts its interaction with the 14-3-3 proteins (19) and promotes its translocation to the nucleus, thereby inducing cell death in neurons by targeting the *bim* gene in mammals (16). In nemotodes, the *Caenorhabditis elegans* MST1 ortholog CST-1 phosphorylates DAF-16 and activates the downstream Daf-2-dependent pathway required for promoting life span extension (20). Knockdown of the *C. elegans* MST1 accelerates aging and reduces life span. In contrast, overexpression of CST-1 delays tissue aging (16,20).

In this study, we employ kinetic analysis to investigate the role of the various MST1 domains in regulating the phosphorylation of the FoxO and histone H2B substrates. We also identify an autophosphorylation region in a C-terminal domain of MST1 that functions to modulate its activity toward its respective substrates. Finally, we investigate the effect of C-terminal MST1 phosphorylation and dimerization on FoxO phosphorylation

MATERIALS AND METHODS

Commercial Reagents

Recombinant histone H2B (New England Biolabs) from human was used as a MST1 substrate at a concentration of 1 mg/mL. Radiolabeled [γ-^{32}P]ATP (3000 Ci/mmol) was purchased from Perkin-Elmer Life Sciences. All other reagents were purchased from Sigma Pharmaceuticals.

Protein Cloning, Expression, and Purification

(i) MST1—Full-length human MST1 (residues 1–487) and the kinase domain (residues 1–334) were PCR amplified from clone 7939613 (Open Biosystems) and subcloned into a modified baculovirus vector, pac-his-tev, which is under the polyhedrin promoter (21). The vector was transfected into SF9 cells using the baculogold transfer vector, and the resulting virus was amplified. Thirty milliliters of the amplified virus was used to infect an sf21 cell suspension, and the cells were harvested 48 h postinfection. MST1(1–334) and MST1-(1–487), both containing an N-terminal six-His tag, were purified using Ni-NTA affinity chromatography followed by gel filtration using a Superdex S200a analytical column. Cells were lysed in wash buffer [50 mM Tris (pH 8.0), 400 mM NaCl, 2 mM imidazole, and 1 mM β-mercaptoethanol] supplemented with protease inhibitors. The clarified supernatant was applied to Ni^{2+}-nitrilotriacetic acid agarose (Qiagen) and washed thoroughly with wash buffer supplemented with 10 mM imidazole. MST1 protein was eluted with 25 mM Hepes (pH 7.5), 100 mM NaCl, and 200 mM imidazole. The eluted protein was concentrated and loaded onto a Superdex 200 (Pharmacia) gel filtration column pre-equilibrated with 25 mM Hepes (pH 7.5) and 100 mM NaCl. The eluted fractions were pooled and concentrated to 2 mg/ mL, aliquoted to avoid repetitive freeze–thaw cycles, and finally flash-frozen and stored at −80 °C. We obtained 5 mg of protein per liter of SF21 cells for each protein construct.

Full-length pac-his-tev-MST1 kinase was used as a template to prepare the S340A/T346A/T348A triple mutant as well as the deletion mutant MST1(1–380). All mutageneses were performed using the site-directed mutagenesis method as described by Kundel (QuickChange site-directed mutagenesis, Strategene) (22). Viruses were prepared for each of the mutants, and the proteins were expressed and purified as described above.

(ii) FoxO—The forkhead domain of FoxO1 (residues 151–266) was cloned into a pETDuet-1 vector containing a gene encoding a six-His tag and the gene for yeast SMT3, a ubiquitin-like protein of the small ubiquitin-related modified (23) [SUMO (24)] family, upstream of the FoxO1 protein region. Overnight expression at 15 °C in BL21(DE3) LysS (Novagen) yielded a six-His SUMO–FOXO fusion protein that was purified via chromatography on Ni-NTA agarose; the His-SUMO tag was cleaved by treatment with ULP1 (ubiquitin-like-specific protease 1) (25), and additional chromatography was carried out using SP-Sepharose ion exchange and Superdex-75 gel filtration. The protein was concentrated to 8 mg/mL for storage at −70 °C.

(iii) Bacterial Expression of InactiVe MST1 Kinase—Efforts to express the active full-length or kinase domain of MST1 using bacterial expression systems were unsuccessful. In contrast, we were able to prepare MST1 constructs in bacteria harboring an inactivating K59R mutation (interfering with ATP binding). DNA encoding the truncated version of MST1, residues 1–334 encompassing the kinase domain, and residues 1–380, a dimer defective deletion mutant harboring the K59R mutation, were cloned into the pET 28a vector (Novagen). DNA encoding the kinase dead versions of MST1 were transformed into BL21(DE3) cells for overnight expression at 18 °C. Cells were lysed in wash buffer supplemented with protease inhibitors, and the clarified supernatant was purified by Ni-NTA affinity chromatography followed by gel filtration as described for the baculovirus-prepared proteins.

(iV) C-Terminal MST1 Fragments—We designed multiple gluthathione *S*-transferase (GST) constructs starting from residue 334 on MST1 (the end of the kinase domain) toward the C-terminus encompassing the proposed autoinhibitory and dimerization domain. Each of these constructs was cloned into the pGEX4T3 vector, overexpressed in BL21(DE3) cells, and purified using GST binding beads using 50 mM phosphate buffer (pH 7.0), 300 mM NaCl, and 1 mM DTT as the wash buffer. The fractions were eluted using 25 mM glutathione dissolved in wash buffer, and the eluted protein was further purified using gel filtration chromatography as described above.

Protein Kinase Assay

Kinase assays were performed using[γ-^{32}P]ATP, and the incorporation of labeled phosphate onto the substrates FOXO and histone H2B was monitored. Kinase assays were performed using kinase buffer containing 10 mMTris (pH 7.5), 10 mM $MgCl_2$, 1 mM dithiothreitol (DTT), 1mM PMSF (phenylmethanesulfonyl fluoride), and a cocktail containing phosphatase inhibitor. Five microcuries of labeled[γ-^{32}P]ATP and a final ATP concentration of 200 μM was used for each reaction. To determine the kinetic rate constants for each substrate, we monitored the incorporation of radiolabeled ^{32}P phosphate onto each of the individual substrates (H2B and FoxO1). To quantify the signal, we created a standard curve for each substrate recording 100% of the signal. For the purposes of determining the kinetic constants, the kinase reactions were performed from 5 to 20 min and at enzyme concentrations from 2 to 500 nM to determine the linear range. The optimal concentration of full-length MST1 and MST1(1–334) was determined to be 10 nM. The reactions were initiated by addition of the respective enzymes, and the reaction was performed in a total final volume of 25 μL. Under these conditions, all initial velocity reactions utilize less than 10% of the substrate. All reaction mixtures were incubated at room temperature and then stopped with SDS gel loading dye; subsequently, samples were heated for 3 min and loaded onto a 16% Tris-gylcine gel (Novagen). The bands were visualized using high-sensitivity Kodak film, and the results were quantified using ImageJ. All kinetic studies were performed in triplicate, and the kinetic data were fit to equations using the iterative minimum χ^2 nonlinear regression method of Leatherbarrow and converted into double-reciprocal Linewaever–Burk plots (26). The data were fitted to the Micheles–Menten equation: $1/\nu = (K_M/V_{max})(1/[S])+1/V_{max}$, where $1/V_{max}$ is the y intercept with k_{cat} being equal to $V_{max}/[E]t$ and the x intercept equal to $1/K_M$ (27).

Analytical Ultracentrifugation

Sedimentation equilibrium experiments were performed with a Beckman Optima XL1 ultracentrifuge at 4 °C, and in a buffer containing 20 mM Hepes, 100 mM NaCl, and 1 mM β-mercaptoethanol. The protein samples were loaded in four-sector 12 mm centerpieces. The native full-length MST1 and the deletion mutant MST1(1–380) samples were analyzed at concentrations of 0.15, 0.30, and 0.60 mg/mL, and each protein concentration was analyzed at centrifugation speeds of 18000, 20000, and 24000 rpm. Samples were detected using absorption optics at 280 nm, and equilibrium was assessed by comparing successive scans using MATCH. Raw data were edited using REEDIT, and data analysis was carried out using NONLIN. Global data fits were carried out to calculate the effective molecular weight in an ideal single-species model. Models for associating molecules used the calculated values from the monomer molecular weight and fitted to dissociation constants. The quality of the fits was assessed by examining residuals and minimizing the fit variance.

Probing T183 Activation Loop Phosphorylation

The following procedure was employed to probe the MST1 threonine 183 phosphorylation status of the various MST1 constructs. In vitro kinase assays were performed at an enzyme concentration of 1 μM and an ATP concentration of 200 μM. Equimolar amounts of MST-FL, MST-KD, MST-KD K59, R, MST1-KD/RR, and MST-FL (TM) were incubated with ATP in kinase buffer. The reaction was stopped after 20 min with the addition of SDS–PAGE loading dye. The samples were subsequently boiled, subjected to Western blot analysis, and probed using phospho-specific T183 antibody (Cell Signaling Inc.).

RESULTS

Preparation of ActiVe Recombinant MST1 Kinase

To study MST1 kinase activity in vitro, we prepared several recombinant MST1 protein constructs (Figure 1A). Attempts to prepare active MST1 protein constructs in bacteria were unsuccessful; however, the active MST1 kinase domain (MST1-KD, residues 1–334) and the full-length protein (MST1-FL) could readily be prepared in an SF21 cell baculovirus system (Figure 1B). These proteins were expressed as N-terminal six-His fusion proteins and purified to homogeneity using Ni-NTA affinity and gel filtration chromatography (Figure 1B).

The forkhead domain of FoxO1 (residue 151–266) and full-length histone H2B were used as MST1 substrates in this study (Figure 1C). The ability of the purified MST1-FL enzyme to phosphorylate histone H2B and FoxO was confirmed as shown in Figure 1C. The ability of MST1-FL to phosphorylate FoxO in the absence and presence of cognate Daf-16 response element DNA was also tested, and we found that MST1-FL fails to phosphorylate the DNA-bound form of FoxO1 (Figure 1D). This data show that DNA binding and MST1-mediated phosphorylation of FoxO1 are competitive, consistent with the fact that serine residues in FoxO1 that serve as MST1 substrates are blocked upon DNA binding. Our results also lead to the conclusion that MST1 is unlikely to influence the transcriptional activity of FoxO protein that is already associated with DNA and thus unlikely to relieve the transcriptional activity of FoxO proteins.

Phosphorylation of FoxO1 and Histone H2B by MST1 Kinase

To understand the kinetics of FoxO1 phosphorylation by MST1 kinase, we carried out Micheles–Menten kinetics. The initial velocity for the incorporation of [γ-^{32}P]ATP was measured against FoxO1 concentration, and the data were plotted in the form of a double-reciprocal plot. Figure 2A shows the Lineweaver–Burk plot comparing the activity of full-length MST1 and the kinase domain toward FoxO1. A comparison of the data shows that while the relative k_{cat} values for the phosphorylation of FoxO1 are similar for the two MST1 protein constructs, MST1-FL has a 7-fold lower K_M for FoxO1 compared to that of MST1-KD (Figures 2A,D,E and S1A,B). This decreased K_M value exhibited by MST1-FL suggests that the C-terminal domain of the MST1 kinase contributes to FoxO1 association. A comparison ofthe catalytic efficiency (k_{cat}/K_M) of the two MST1 constructs toward the FoxO1 substrate also shows an 6-fold greater catalytic efficiency of the full-length enzyme over the kinase domain. This observation correlates well with the fact that full-length MST1 kinase, and not the caspase-cleaved MST1 kinase domain, phosphorylates FoxO1 in the cytosol to relieve FoxO1 repression by the 14-3-3 adaptor protein.

To compare histone H2B as a substrate for MST1, we characterized the activity of the full-length and kinase domain of MST1 toward H2B using substrate kinetics essentially as described for the FoxO1 substrate. The resulting double-reciprocal plot comparing the activity of MST1-FL and MST1-KD toward histone H2B is shown in panels b and c of Figure 2, and the steady state parameters are summarized in Figure 2D. Interestingly, the MST1 kinase domain shows k_{cat} and K_M values that are 10-fold greater and 4-fold lower,respectively, than those of the full-length kinase toward histone H2B (Figures 2D,F and S1C,D). As a result, the overall catalytic efficiency of MST1-KD toward histone H2B is 30 times higher than that of MST1-FL. This is in contrast to the FoxO1 substrate, which is turned over 6-fold more efficiently by MST1-FL. These results with the histone H2B substrate are also consistent with the fact that the caspase-cleaved from of MST1 in the nucleus is the form that phosphorylates nuclear histone H2B most efficiently.

C-Terminal Autophosphorylation of MST1 Kinase

While performing in vitro kinase assays, we observed that the autophosphorylation signal of MST1-FL was much more pronounced than equimolar amounts of MST1-KD (Figure 3A). This was particularly unexpected given that most of the known phosphorylation sites of MST1 were mapped to the N-terminal kinase domain (11). The differential ability of MST1-FL to autophosphorylate itself prompted us to map the sites of phosphorylation and determine whether this phosphorylation regulates kinase activity or some other aspects of MST1 function. To find the region of autophosphorylation, we constructed GST-tagged C-terminal fragments starting at different points after the kinase domain and extending to the C-terminal end of the protein (Figure 1A). The three GST-tagged C-terminal MST1 constructs prepared were 338-end, 354-end, and 388-end, and each was purified by affinity chromatography followed by gel filtration and subjected to in vitro kinase assays using MST1-FL. The results of the assay are shown in Figure 3B and demonstrate that only the largest of three fragments spanning the MST1 C-terminal region, 338-end, is a substrate for phosphorylation. These results indicate that the C-terminal phosphorylation sites of MST1 lie between residues 338 and 354. We next prepared a GST construct spanning residues 338–354 and also systematically mutated the serines and threonines in this region but found that single-site mutations had no apparent effect on MST1 C-terminal autophosphorylation (data not shown). A triple mutant was prepared containing the S340A, T346A, and T348A substitutions, and we found that this mutant was not detectably phosphorylated (Figure 3C). The autophosphorylation activity of intact MST1 has been noted previously (28), where the authors reported that the full-length form of MST1 and the 41 kDa species strongly autophosphorylate whereas a 36 kDa fragment of MST1 autophosphorylates very weakly. The possible site was attributed to S327, which is adjacent to the caspase-3 cleavage site DEVD^{326} of MST1. However, our results indicate that the phosphorylation region is around the second caspase cleavage site TMTD^{349}. Collectively, the data presented here suggest that MST1 autophosphorylation sites are located outside the activation loop and within the regulatory region between the two caspase cleavage sites within the region of amino acids 326–354.

The current mechanistic evidence in the literature supports the fact that MST1 kinase exists as a dimer in solution and that autophosphorylation is an intermolecular event, where an adjacent MST1 molecule phosphorylates its partner (11). In light of this model, we carried out kinetic experiments to determine the efficiency of N- and C-terminal autophosphorylation by MST1. The kinase dead form of MST1 purified from bacteria was used to monitor N-terminal phosphorylation, and the GST–MST1(338-end) construct was used to monitor C-terminal phosphorylation. Panels D and E of Figure 3 (and Figure S1E,F) compare plots of substrate concentration verses initial velocity for the N- and C-terminal MST1 substrates and reveal that MST1 exhibits an 10-foldhigher k_{cat} but a 20-fold higher K_M for the N-terminal domainrelative to the C-terminal domain (Figure 3F). Together, the catalytic efficiency of MST1 is 15-fold higher for the N-terminal domain relative to the C-terminal domain. This demonstrates that N-terminal autophosphorylation is more efficient than C-terminal autophosphorylation by MST1 and that this phosphorylation can occur in trans.

Dimerization Properties of MST1

Creasy et al. used immunoprecipitates of epitope-tagged MST1 from transfected cells and a yeast two-hybrid assay to show that MST self-associates (5), and a recent solution structure of C-terminal residues 432–480 of MST1 demonstrates that this region forms a symmetric homodimer (29). Given the dimerization properties of MST1, we addressed its role in the phosphorylation of MST1 substrates, including proximal C-terminal autophosphorylation. We first carried out analytical ultracentrifugation (AU) on MST1-FL and the dimerization domain-deleted construct of MST1(MST1-KD/RR, residues 1–380) to determine the oligomerization state of full-length MST1 and its deletion mutant. This analysis was carried out at three different centrifugation speeds and three different protein concentrations for each of the two forms of the protein. The results of a global analysis of the data are shown in panels A and B of Figure 4 and demonstrate that full-length MST1 exists as a homogeneous homodimer, while the C-terminal deletion mutant exists as a homogeneous monomer. This result is consistent with previous findings and suggests that full-length MST1 dimers exist in vivo.

To determine the role of the MST1 dimerization domain in MST1-mediated phosphorylation of FoxO1, we assayed the FoxO1 phosphorylation activity of the dimerization defective MST1-KD/RR protein construct for comparison with MST1-FL and MST1-KD (Figures 4C and S2A,B). Surprisingly, we find that the dimerization defective mutant not only has a reduced level of binding toward FoxO, with a K_M value that is even higher than that of MST1-KD, but also has a lower catalytic efficiency, by 50-fold. In addition, the phosphorylation defective MST1-FL mutant also has a reduced phosphoryaltion activity toward FoxO1, by 6-fold. Taken together, these data demonstrate that MST1 dimerization and C-terminal autophosphorylation both contribute to FoxO1 phosphorylation with dimerization playing a more significant role.

AutoactiVation Status of MST1

To probe the autoactivation status of MST1, we probed the extent of autophosphorylation on threonine 183 of the activation loop using a phospho-specific antibody. Results shown in Figure S3 indicate that each of the MST1 constructs used in this study, except for the kinase dead (K59R) mutant, is autophoshorylated, and there is a slightly enhanced signal for MST-FL and MST-KD/RR as compared to MST-KD and MST-FL (TM). These results indicate that MST1 regulatory activities within the region C-terminal to the kinase domain do not have a dominant effect on the autoactivation status of MST1.

DISCUSSION

Two physiological substrates of the MST1 kinase, FoxO and histone H2B, have been previously identified (12,16). While the full-length MST1 enzyme is thought to be the predominant form that phosphoryaltes FoxO1 in the cytosol, the caspase-cleaved kinase domain of MST1 is thought to be the predominant form that phosphorylates histone H2B in the nucleus. In this study, we analyze the ability of the full-length and caspase-cleaved form of MST1 to phosphorylate its substrates and find that that while the full-length enzyme prefers the FoxO1 susbstrate, the caspase-cleaved form prefers the histone H2B substrate. These results indicate that the C-terminal domain of MST1 is versatile and can exhibit stimulatory or inhibitory activities depending on the particular substrate. These results are consistent with where these forms of the enzyme normally function and may serve to prevent MST1-mediated phosphorylation of FoxO1 in the nucleus and histone H2B in the cytoplasm.

In this study, we also report that a regulatory region of MST1 contains at least three autophosphorylation sites and that these sites affect MST1 funciton. Previous studies have noted an enhanced phosphorylation of the full-length MST1 protein that correlates with complete activation of the kinase (28). To reconcile these findings, we carried out deletion and mutational analysis demonstrating that the region spanning residues 340–350 within the C-terminal regulatory domain is the site of C-terminal autophosphorylation by MST1. We also show that mutation of the three phosphorylation sites within this region (S340/T346/T348) reduces MST1 activity toward the FoxO1 substrate, implicating a role of MST1 C-teminal autophosphoryaltion in MST1 substrate activity. These C-terminal MST1 phosphorylation sites are in the proximity of the $TMTD^{349}$ caspase cleavage site created by caspase-6/7 to generate a 41 kDa MST1 species. In response to certain stimuli like oxidative stress, selective phosphorylation around this caspase site may lead to inhibition of caspase cleavage activity, preventing the release of the 41 kDa fragment leading to the retention of the MST1 in the cytoplasm. This, in turn, makes MST1 available for cytosolic FoxO phosphorylation and activation as opposed to nuclear histone H2B phosphorylation. A precedent for phospho-inhibition of caspase cleavage has been demonstrated for I-kBβ regulation (30).

The N-terminal kinase domain of MST1 has previously been shown to be a site of autophosphorylation (11). To improve our understanding of the relative preference of the N- and C-terminal MST1 autophosphorylation events, we carried out a kinetic analysis and determined the catalytic efficiency of these "pseudosubstrates" for MST1. Our results demonstrate that phosphorylation of the kinase domain has a higher k_{cat} than the regulatory domain while the regulatory domain had a lower K_M. This is consistent with a role of N-terminal autophoshorylation in activation of protein phosphorylation with C-terminal autophosphorylation playing a more regulatory role involving competitive binding with substrate. For example, the phosphorylation of histone H2B at serine 14 by the caspase-cleaved form of MST1 is closely linked with the onset of apoptosis (12). Under conditions of stress, the caspase-cleaved form of MST1 is nuclear-localized, and in this truncated form, it phosphorylates histone H2B. However, under normal conditions, any full-length MST1 shuttling between the nucleus and cytoplasm could be prevented from accidental phosphorylation of histone H2B by the C-terminal domain which occupies the binding pocket adopted by histone H2B and blocks access. The low efficiency of full-length MST1 toward histone H2B phosphorylation may therefore serve as a safeguard mechanism against promiscuous basal phosphorylation of histone H2B by full-length MST1 and prevent the triggering of unregulated apoptosis. However, under apoptotic conditions, the C-terminal block is removed by caspase cleavage, giving full access to histone H2B and facilitating phosphorylation. A similar level of regulation has also been observed in other kinases like PAK, where the autoinhibitory segment is located in the N-terminal region of the protein (31).

The extreme C-terminal region of MST1 has been reported to participate in protein dimerization and also to mediate MST1 activity by interacting with protein binding partners such as NORE (novel Ras effector) and other RASSF binding isoforms (10). These proteins are adaptor proteins and bind specifically to GTP-liganded forms of Ras and have been shown to be involved in tumor suppression by inhibiting cell growth in a subset of tumor cell lines (32). We investigated the effect of deleting the C-terminal dimerization domain of MST1 on FoxO1 phosphorylation activity. We first carried out analytical ultracentrifugation studies and confirmed that in the absence of the C-terminal dimerization domain of MST1 loses its ability to dimerize and exists as a homogeneous monomer. Our data on FoxO1 phosphorylation reveal that deletion of the C-terminal dimerization domain significantly lowers the activity of MST1 toward FoxO1 phosphorylation, demonstrating that this dimerization plays an important role in MST1-mediated phosphorylation of FoxO1. We also demonstrate that phosphorylation within the MST1 regulatory region also stimulates FoxO1 phosphorylation, although not as potently as MST1 dimerization. Therefore, an interplay of both dimerization and phosphorylation is important in regulating MST1 phosphorylation of FoxO proteins.

Together, we have carried out a detailed analysis of MST1 kinase activity toward both its nuclear histone H2B and cytosolic FoxO1 substrates, and we show that a C-terminal regulatory domain harboring autophosphorylation sites and an extreme C-terminal dimerization domain play key roles in regulating MST1-mediated cellular apoptosis.

Supplementary Material

Refer to Web version on PubMed Central for supplementary material.

Acknowledgments

We thank Dr. Thanuja Krishnamoorthy for her initial help in assisting with the kinase assays, Manqing Hong for her assistance with the ultracentrifugation, and the Wistar Protein Expression facility for help with protein production.

References

1. Creasy CL, Chernoff J. Cloning and characterization of a human protein kinase with homology to Ste20. J Biol Chem 1995;270:21695–21700. [PubMed: 7665586]
2. Pombo CM, Force T, Kyriakis J, Nogueira E, Fidalgo M, Zalvide J. The GCK II and III subfamilies of the STE20 group kinases. Front Biosci 2007;12:850–859. [PubMed: 17127342]
3. Dan I, Watanabe NM, Kusumi A. The Ste20 group kinases as regulators of MAP kinase cascades. Trends Cell Biol 2001;11:220–230. [PubMed: 11316611]
4. Zhao ZS, Manser E. PAK and other Rho-associated kinases: Effectors with surprisingly diverse mechanisms of regulation. Biochem J 2005;386:201–214. [PubMed: 15548136]
5. Creasy CL, Ambrose DM, Chernoff J. The Ste20-like protein kinase, Mst1, dimerizes and contains an inhibitory domain. J Biol Chem 1996;271:21049–21053. [PubMed: 8702870]
6. de Souza PM, Lindsay MA. Mammalian Sterile20-like kinase 1 and the regulation of apoptosis. Biochem Soc Trans 2004;32:485–488. [PubMed: 15157167]
7. Ura S, Masuyama N, Graves JD, Gotoh Y. MST1-JNK promotes apoptosis via caspase-dependent and independent pathways. Genes Cells 2001;6:519–530. [PubMed: 11442632]
8. Lee KK, Ohyama T, Yajima N, Tsubuki S, Yonehara S. MST, a physiological caspase substrate, highly sensitizes apoptosis both upstream and downstream of caspase activation. J Biol Chem 2001;276:19276–19285. [PubMed: 11278283]
9. Lee KK, Murakawa M, Nishida E, Tsubuki S, Kawashima S, Sakamaki K, Yonehara S. Proteolytic activation of MST/Krs, STE20-related protein kinase, by caspase during apoptosis. Oncogene 1998;16:3029–3037. [PubMed: 9662336]
10. Praskova M, Khoklatchev A, Ortiz-Vega S, Avruch J. Regulation of the MST1 kinase by autophosphorylation, by the growth inhibitory proteins, RASSF1 and NORE1, and by Ras. Biochem J 2004;381:453–462. [PubMed: 15109305]
11. Glantschnig H, Rodan GA, Reszka AA. Mapping of MST1 kinase sites of phosphorylation. Activation and auto-phosphorylation. J Biol Chem 2002;277:42987–42996. [PubMed: 12223493]
12. Cheung WL, Ajiro K, Samejima K, Kloc M, Cheung P, Mizzen CA, Beeser A, Etkin LD, Chernoff J, Earnshaw WC, Allis CD. Apoptotic phosphorylation of histone H2B is mediated by mammalian sterile twenty kinase. Cell 2003;113:507–517. [PubMed: 12757711]
13. Luger K, Mader AW, Richmond RK, Sargent DF, Richmond TJ. Crystal structure of the nucleosome core particle at 2.8 Å resolution. Nature 1997;389:251–260. [PubMed: 9305837]
14. Luger K, Rechsteiner TJ, Flaus AJ, Waye MM, Richmond TJ. Characterization of nucleosome core particles containing histone proteins made in bacteria. J Mol Biol 1997;272:301–311. [PubMed: 9325091]
15. Ajiro K. Histone H2B phosphorylation in mammalian apoptotic cells. An association with DNA fragmentation. J Biol Chem 2000;275:439–443. [PubMed: 10617636]
16. Lehtinen MK, Yuan Z, Boag PR, Yang Y, Villen J, Becker EB, DiBacco S, de la Iglesia N, Gygi S, Blackwell TK, Bonni A. A conserved MST-FOXO signaling pathway mediates oxidative-stress responses and extends life span. Cell 2006;125:987–1001. [PubMed: 16751106]
17. Lam EW, Francis RE, Petkovic M. FOXO transcription factors: Key regulators of cell fate. Biochem Soc Trans 2006;34:722–726. [PubMed: 17052182]
18. Burgering BM, Kops GJ. Cell cycle and death control: Long live Forkheads. Trends Biochem Sci 2002;27:352–360. [PubMed: 12114024]
19. Fu H, Subramanian RR, Masters SC. 14-3-3 proteins: Structure, function, and regulation. Annu Rev Pharmacol Toxicol 2000;40:617–647. [PubMed: 10836149]
20. Baumeister R, Schaffitzel E, Hertweck M. Endocrine signaling in *Caenorhabditis elegans* controls stress response and longevity. J Endocrinol 2006;190:191–202. [PubMed: 16899554]

NIH-PA Author Manuscript

NIH-PA Author Manuscript

21. Roy P. Use of baculovirus expression vectors: Development of diagnostic reagents, vaccines and morphological counterparts of bluetongue virus. FEMS Microbiol Immunol 1990;2:223–234. [PubMed: 2178355]

22. Braman J, Papworth C, Greener A. Site-directed mutagenesis using double-stranded plasmid DNA templates. Methods Mol Biol 1996;57:31–44. [PubMed: 8849992]

23. Takahashi Y, Iwase M, Konishi M, Tanaka M, Toh-e A, Kikuchi Y. Smt3, a SUMO-1 homolog, is conjugated to Cdc3, a component of septin rings at the mother-bud neck in budding yeast. Biochem Biophys Res Commun 1999;259:582–587. [PubMed: 10364461]

24. Bossis G, Melchior F. SUMO: Regulating the regulator. Cell Div 2006;1:13. [PubMed: 16805918]

25. Li SJ, Hochstrasser M. A new protease required for cell-cycle progression in yeast. Nature 1999;398:246–251. [PubMed: 10094048]

26. Leatherbarrow, RJ. GraFit. Erithacus Software Ltd; Horley, U.K: 2001.

27. Segel, IH. Enzyme Kinetics, behavior and analysis of rapid equilibrium and steady-state enzyme systems. John Wiley & Sons; New York: 1993.

28. Graves JD, Draves KE, Gotoh Y, Krebs EG, Clark EA. Both phosphorylation and caspase-mediated cleavage contribute to regulation of the Ste20-like protein kinase Mst1 during CD95/Fas-induced apoptosis. J Biol Chem 2001;276:14909–14915. [PubMed: 11278782]

29. Hwang E, Ryu KS, Paakkonen K, Guntert P, Cheong HK, Lim DS, Lee JO, Jeon YH, Cheong C. Structural insight into dimeric interaction of the SARAH domains from Mst1 and RASSF family proteins in the apoptosis pathway. Proc Natl Acad Sci USA 2007;104:9236–9241. [PubMed: 17517604]

30. Barkett M, Xue D, Horvitz HR, Gilmore TD. Phosphorylation of IκB-α inhibits its cleavage by caspase CPP32 in vitro. J Biol Chem 1997;272:29419–29422. [PubMed: 9367996]

31. Lei M, Lu W, Meng W, Parrini MC, Eck MJ, Mayer BJ, Harrison SC. Structure of PAK1 in an autoinhibited conformation reveals a multistage activation switch. Cell 2000;102:387–397. [PubMed: 10975528]

32. Avruch J, Praskova M, Ortiz-Vega S, Liu M, Zhang XF. Nore1 and RASSF1 Regulation of Cell Proliferation and of the MST1/2 Kinases. Methods Enzymol 2005;407:290–310. [PubMed: 16757333]

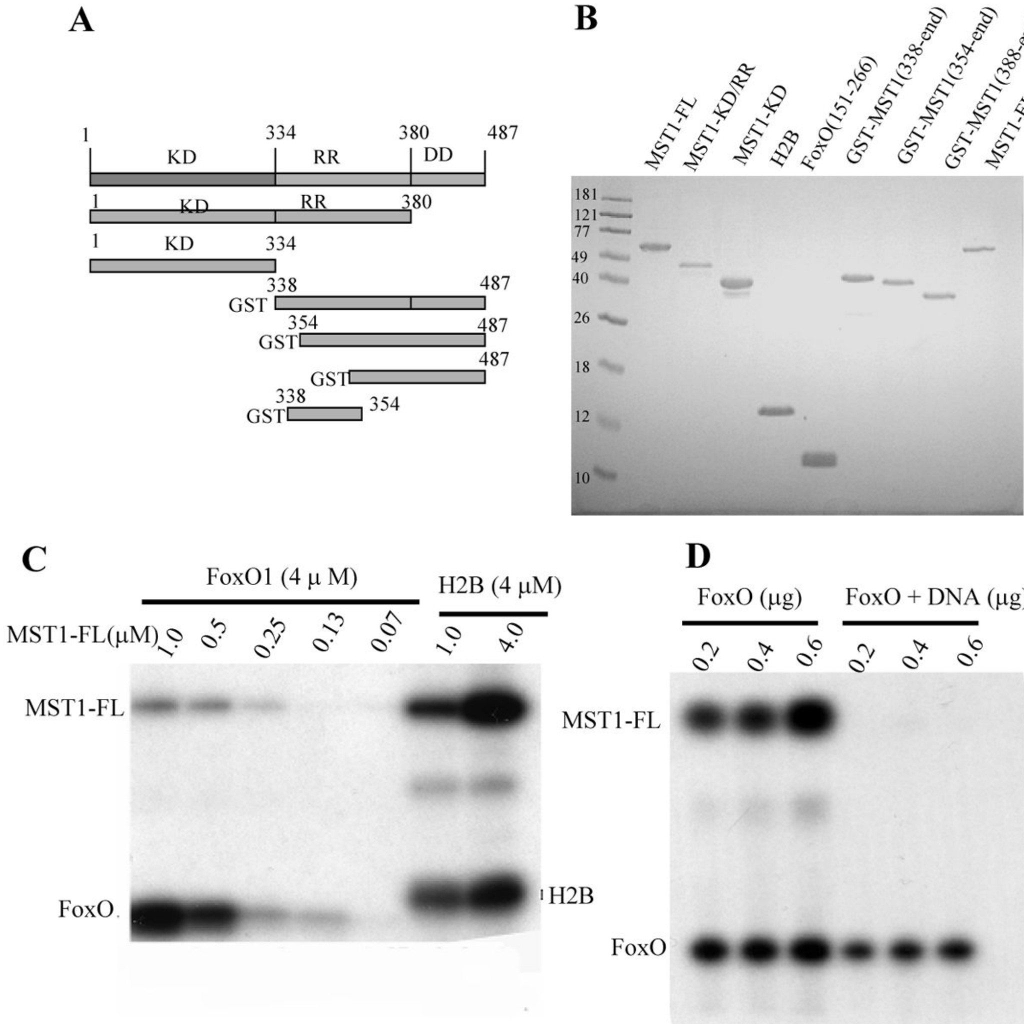

Figure 1.

MST1 preparation and characterization. (A) The construct designs for the various protein fragments of MST1 used for this study are depicted. The various domains are abbreviated as follows: KD, kinase domain; RR, regulatory region; and DD, dimerization domain. (B) SDS page gel of the various recombinant protein constructs used in this study. The abbreviations are as follows: MST1-FL, full-length MST1; MST1-KD/RR, MST1 kinase with the regulatory region, spanning residues 1–380; and MST1-FL (TM), MST1-FL triple mutant with residues S340, T346, and T348 mutated to alanine. (C) Autoradiography gel showing the activity of MST1 toward phosphorylation of its substrates, FoxO1 and histone H2B. The signal depicted is the incorporation of the γ-^{32}P label onto FoxO and histone H2B. The autophosphorylation signal of MST1 is also visible as indicated. (D) Autoradiograph showing the effect of DNA binding on the phosphorylation activity of FoxO1 by MST1-FL in the presence and absence of its cognate DNA, the Daf-16 binding element

NIH-PA Author Manuscript
NIH-PA Author Manuscript

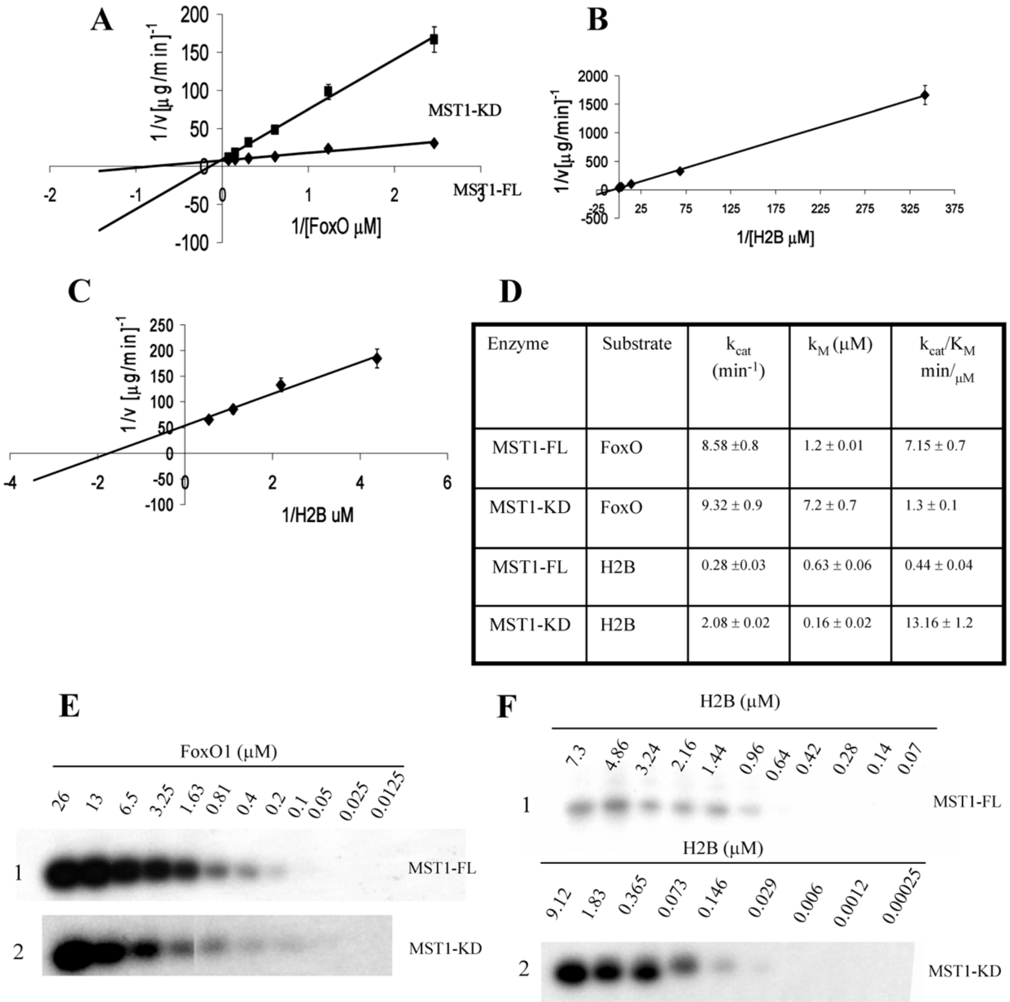

Enzyme	Substrate	k_{cat} (min^{-1})	k_M (μM)	k_{cat}/K_M min/μM
MST1-FL	FoxO	8.58 ±0.8	1.2 ± 0.01	7.15 ± 0.7
MST1-KD	FoxO	9.32 ± 0.9	7.2 ± 0.7	1.3 ± 0.1
MST1-FL	H2B	0.28 ±0.03	0.63 ± 0.06	0.44 ± 0.04
MST1-KD	H2B	2.08 ± 0.02	0.16 ± 0.02	13.16 ± 1.2

Figure 2.

Kinetic analysis of MST1 protein constructs. (A) Lineweaver–Burk plot comparing the activity of MST1-FL and the kinase domain (MST1-KD) toward FoxO1. (B) Lineweaver–Burk plot depicting the activity of MST-KD toward histone H2B. (C) Lineweaver–Burk plot depicting the activity of MST1-FL toward histone H2B. (D) Summary of the various steady state parameters for the plots shown in panels A–C. (E and F) Autoradiography gel showing the activity of MST1-FL and MST1-KD toward FoxO1 and histone H2B, respectively. The gel shows the incorporation of the γ-^{32}P label as a function of substrate concentration. All reactions were carried out for 15 min and then stopped with the addition of SDS–PAGE loading buffer.

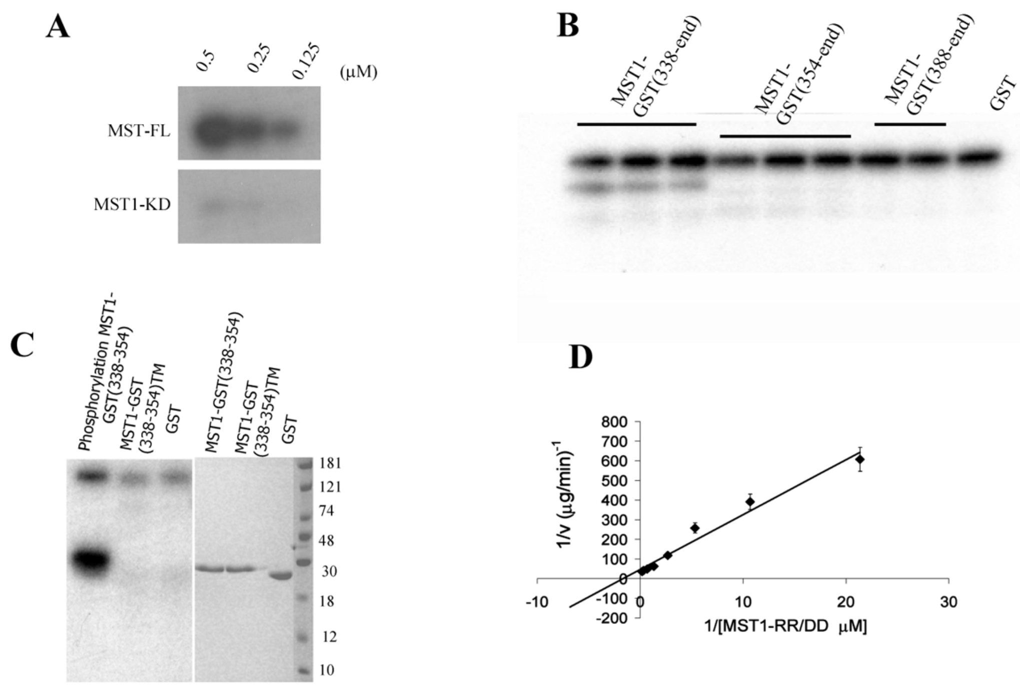

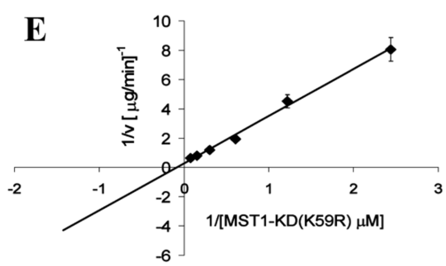

F

Substrate	k_{cat} (min^{-1})	K_M (μM)	k_{cat}/K_M min/μM
MST1-KD	2.13 ± 0.2	11.3 ± 1.3	5.3 ± 0.5
MST1-RR/DD	0.214 ± 0.02	0.6 ± 0.06	0.33 ± 0.03

Figure 3.

Autophosphorylation of MST1. (A) Autoradiogarphy comparing the autophosphorylation activity of equimolar amounts of MST1-FL and MST1-KD. (B) Autoradiogarphy showing the autophosphorylation activity of various GST-tagged MST1 fragments. MST-FL was used as the enzyme to monitor γ-^{32}P incorporation. (C) Autoradiogarphy and SDS page gel of the GST-tagged phosphorylated region (residues 338–354) of wild-type MST1 and the TM mutant. (D) Lineweaver–Burk plot depicting the phosphorylation of MST1-FL toward a MST1 C-terminal region spanning residues 338–487 that encompasses the RR and DD. (E) Lineweaver–Burk plot depicting N-terminal KD domain phosphorylation of MST1. A kinase dead version of the enzyme harboring a K59R mutation was used as a substrate. (F) Summary of the various steady state parameters for plots shown in panels E and F.

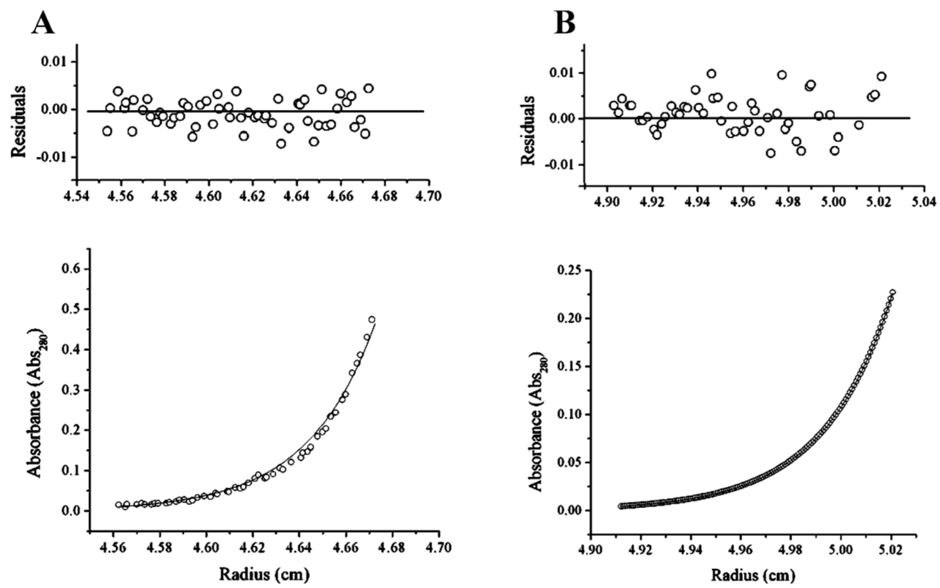

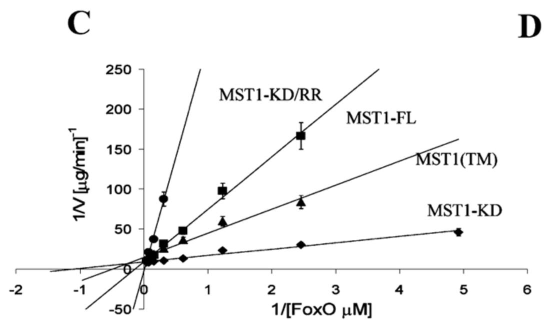

D

Enzyme	k_{cat} (min^{-1})	K_M (μM)	k_{cat}/K_M min/μM
MST1-KD/RR	0.3 ± 0.03	13.8 ± 1.4	0.02 ± 0.002
MST1(TM)	8.3 ± 0.8	6.12 ± 0.6	1.4 ± 0.1
MST1-FL	8.58 ± 0.8	1.2 ± 0.1	7.15 ± 0.7
MST1-KD	9.32 ± 0.9	7.2 ± 0.7	1.3 ± 0.1

Figure 4.
Effect of MST1 dimerization on kinase activity. (A) Sedimentation equilibrium data for MST1-FL were fitted with data from nine curves (three protein concentrations at three centrifugation speeds). A representative run at a centrifugation speed of 20000 rpm and protein concentration of 0.3 mg/mL is shown. The plots represent a best fit to a single-dimeric species model to which all nine curves were fitted. The bottom panel shows the experimental data (O) with the calculated fits (–). The top panel depicts the residuals of the fits. (B) Sedimentation equilibrium data for the dimerization deletion construct spanning residues 1–380 of MST1. The experiments was carried out as described for panel A under similar conditions. The plot represents a single-monomeric species model to which all the nine curves were fit. (C) Lineweaver–Burk plot comparing the activity of various MST1 constructs toward FoxO1. Kinetics was performed on both the dimerization deletion mutant (MST1-KD/RR, residues 1–380) and the phosphorylation defective triple mutant MST1 (TM). (D) Summary of the various steady state parameters for the plots shown in panel C.